

1  
2  
3  
4                   Micro/nanoliter droplet extraction by controlling acoustic vortex with  
5  
6  
7   miniwatt  
8  
9

10  
11   Han Zhang<sup>1,2,\*</sup>, Jun Yang<sup>1,2</sup>, Yun Zhou<sup>3,4</sup>, Jianfeng Zheng<sup>4</sup>, Yong Cheng<sup>5</sup>, Bichao Bai<sup>4</sup>, Guoxin  
12  
13   Zhang<sup>6</sup>, Yisheng Lv<sup>7</sup>  
14  
15  
16  
17  
18  
19  
20

21                   <sup>1</sup>CAS Key Laboratory of Noise and Vibration, Institute of Acoustics, Chinese Academy of  
22  
23   Sciences, Beijing 100190, China.  
24

25  
26                   <sup>2</sup>University of Chinese Academy of Sciences, Beijing 100049, China.  
27  
28

29                   <sup>3</sup>The National Center for Nanoscience and Technology, Beijing , 100190, China.  
30  
31

32                   <sup>4</sup>School of Mechanical Engineering, Changzhou University, Changzhou 213164, China.  
33  
34

35                   <sup>5</sup>Institute of Mechanics, School of Civil Engineering & Mechanics, Yanshan University,  
36  
37   Qinhuangdao 066004, PR China.  
38  
39

40                   <sup>6</sup>Al-ion Battery Research Center, Department of Electrical Engineering and Automation,  
41  
42   Shandong University of Science and Technology, Qingdao 266580, China.  
43  
44

45                   <sup>7</sup>State Key Laboratory of Management and Control for Complex Systems, Institute of  
46  
47   Automation, Chinese Academy of Sciences, Beijing 100190, China.  
48  
49

50  
51                   (\*Corresponding author: [zhanghan@mail.ioa.ac.cn](mailto:zhanghan@mail.ioa.ac.cn))  
52  
53  
54  
55  
56  
57  
58  
59  
60  
61  
62  
63  
64  
65

1  
2  
3  
4 **ABSTRACT**  
5

6  
7 Micro/nanoliter droplet is capable of achieving versatile applications with tiny volume and  
8  
9 substantial surface energy, which is a big plus over bulk liquid. Yet, the contradiction of elaborate  
10  
11 manipulation and enough power is still a challenge. Here, we unleash the potential of our miniwatt  
12  
13 aspirators pumping up liquid and creating droplets with the help of acoustic vortex beams, inspired  
14  
15 by the power mechanism that spirals are significant for most mollusks that live in water. These  
16  
17 droplet aspirators produce very large interface deformations by small radiation pressures with orbit  
18  
19 angular momentum from spiral-electrode transducers. The precisely contactless manipulation of  
20  
21 physical, chemical and biological objects at micrometric down to nanometric scales, promises  
22  
23 tremendous development in fields as diverse as microrobotics, nanoreactors, or nanoassemblies.  
24  
25  
26  
27  
28  
29

30  
31 *Keywords:*  
32

33 Micro/nanoliter droplet  
34

35  
36 Miniwatt  
37

38 Vortex beams  
39  
40  
41  
42  
43  
44  
45  
46  
47  
48  
49  
50  
51  
52  
53  
54  
55  
56  
57  
58  
59  
60  
61  
62  
63  
64  
65

1  
2  
3  
4 **1. Introduction**  
5

6  
7 Generation and manipulation of droplets have contributed in many outstanding achievements  
8  
9 in physics, energy, biology, chemistry and material science over the latest few years [1-13]. During  
10 these successful experiences, droplet is prominently capable of achieving versatile applications  
11 with tiny volume and substantial surface energy in comparison with bulk liquid. In this regard, it  
12 is of great value actuated by droplet manipulation in the fields of micro-fluidic, liquid  
13 transportation, droplet-based electric generator, droplet-based printing, single droplet reactor,  
14 multifunctional sensors, etc. Paradoxically, almost without exception to the equipment in  
15 micromanipulation, the more precise they are, the more expensive their cost needs. What is even  
16 more rigorous is that their propelling powers have been inevitably restricted due to their  
17 dimensions. Yet, micro/nanoliter droplet is still a harsh challenge [5] in the process of preparation  
18 and manipulation, particularly precluded from separability and selectivity at the single droplet  
19 level [12-19]. Wave control totally overcame the definition of macroscopic dimensions, which has  
20 been a preeminent tool for micromanipulation dexterously enough at the wavelength level, through  
21 contactless forces and energy from wave motion. Among the pioneers, Lord Rayleigh in 1902 first  
22 put forward the description of radiation pressure when wave propagating in acoustics, optics or  
23 electromagnetism [20]. Then Chu employed the resonance radiation pressure of a set of six-laser  
24 beams to realize the targeted atom captured in three-dimensional viscous confinement [21]. In the  
25 atomic traps, the kinetic energy of the cooled atoms is reduced to a suspended state since  
26 exchanging momentum between photons and atoms. Arthur went a step further to enhance the  
27 gradient radiation pressure through a highly focused beam to demonstrate a single-beam gradient  
28 force trap of dielectric particles for the first reported time and throughout the concept of negative  
29 light pressure due to the gradient force was verified experimentally [22]. Not only extremely tiny  
30  
31  
32  
33  
34  
35  
36  
37  
38  
39  
40  
41  
42  
43  
44  
45  
46  
47  
48  
49  
50  
51  
52  
53  
54  
55  
56  
57  
58  
59  
60  
61  
62  
63  
64  
65

1  
2  
3  
4 objects and ultra-fast processing but also much more advanced equipment in the span-new fields  
5  
6 for broad industrial and medical applications resort to the invention of optical tweezers. Up till  
7  
8 now, acoustic tweezers have emerged as a prominent technique for controlling cell–cell  
9  
10 interactions without deleterious heating while providing more noninvasive, more biocompatible,  
11  
12 higher penetrability in organic tissues than previous techniques [23-26]. The most important thing  
13  
14 is that they verified the contactless and damageless micromanipulation in wavelength level of  
15  
16 three-dimensional acoustic radiation force [27-29]. So, acoustic wave control supplies us a  
17  
18 potential tool [30-32] to breakout the harsh challenge in the preparation and manipulation process  
19  
20 of micro/nanoliter droplets, which is mentioned above.  
21  
22  
23  
24

25  
26 Here, we harness the mechanism to explore a new kind of miniwatt aspirators to pump up  
27  
28 liquid and create droplet(s) via acoustic vortex beams, inspired by the power mechanism that  
29  
30 spirals are significant for most mollusks that live in water [33]. It is the nature hidden in their  
31  
32 power mechanism with the minimum energy consumption [34-36] that a tiny change in polar  
33  
34 angle can result in a huge change in polar radius over a certain value of the spiral coefficient. The  
35  
36 resistance from the flow is transformed into the propulsion by the pressure difference also due to  
37  
38 their spiral structures [37]. Acoustic vortex beams possess both the advantages of the spiral  
39  
40 structures and the advantages of the precise wave control, which perform an astonishing variety of  
41  
42 applications in many dynamic manipulation [7-11]. However, they have not been applied in the  
43  
44 droplet manipulation of steady extracting yet. Based on the effects of acoustic radiation pressure  
45  
46 on two-phase liquid interfaces [38-40] and orbital angular momentum (OAM) transferring from  
47  
48 the spiral waves spinning around a phase singularity [41-43], we achieve this kind of dynamic  
49  
50 manipulation with our smart invention of miniwatt droplet aspirators illustrated in Fig. 1.  
51  
52  
53  
54  
55  
56  
57  
58  
59  
60  
61  
62  
63  
64  
65

1  
2  
3  
4 By the spiral dynamic mechanism of vortex beams, we succeed in resolving the contradiction  
5 of precision and power in wave control. Hence, we present 5 parts to address our miniwatt droplet  
6 aspirators in this paper. (I) We set up the model of our invention in cylindrical coordination as Fig.  
7 2(a) shown and give out the theoretical analyses of the acoustic radiation force and the acoustic  
8 pressure field of spiral-electrode transducer. (II) We obtained the deformations of the two-phase-  
9 liquid interface and then the droplets with wavelength-scale in the experiments designed as Fig.  
10 2(b). (III) We verified our miniwatt power costs in the comparison of transducers with non-spiral  
11 and spiral electrodes (Fig. 3). (IV) We employed Bernonlli theorem to demonstrate the  
12 contribution of OAM transfer to saving power cost, which is benefits to the rotation velocity of  
13 liquid in the upper layer. The pressure of the upper fluid against the lower fluid reduced by the  
14 existence of OAM transfer is illustrated in Fig. 2(b). (V) Finally, we analyze the force of the slant  
15 liquid column produced on the liquid interface when the transducer is slant. The minimum power  
16 of our aspirators is optimized by the slant vortex beam at  $45^\circ$  which realized our further  
17 optimization of the power costs.  
18  
19  
20  
21  
22  
23  
24  
25  
26  
27  
28  
29  
30  
31  
32  
33  
34  
35  
36  
37  
38  
39  
40

## 41 2. Theory models and design methods

42  
43 In this paper, the control of liquid level and droplets mainly depends on the wave control of  
44 acoustic waves. The mechanism of micro/nanoliter droplet aspirators based on vortex beams is  
45 depicted in Fig. 1. The bottom red medium is carbon tetrachloride ( $CCL_4$ ) and the upper blue  
46 region represents the water. Spiral piezoelectric transducer is adopted to produce vortex acoustic  
47 field. Therefore, the  $CCL_4$  droplet could be manipulated by the acoustic radiation force.  
48  
49  
50  
51  
52  
53  
54  
55  
56  
57  
58  
59  
60  
61  
62  
63  
64  
65

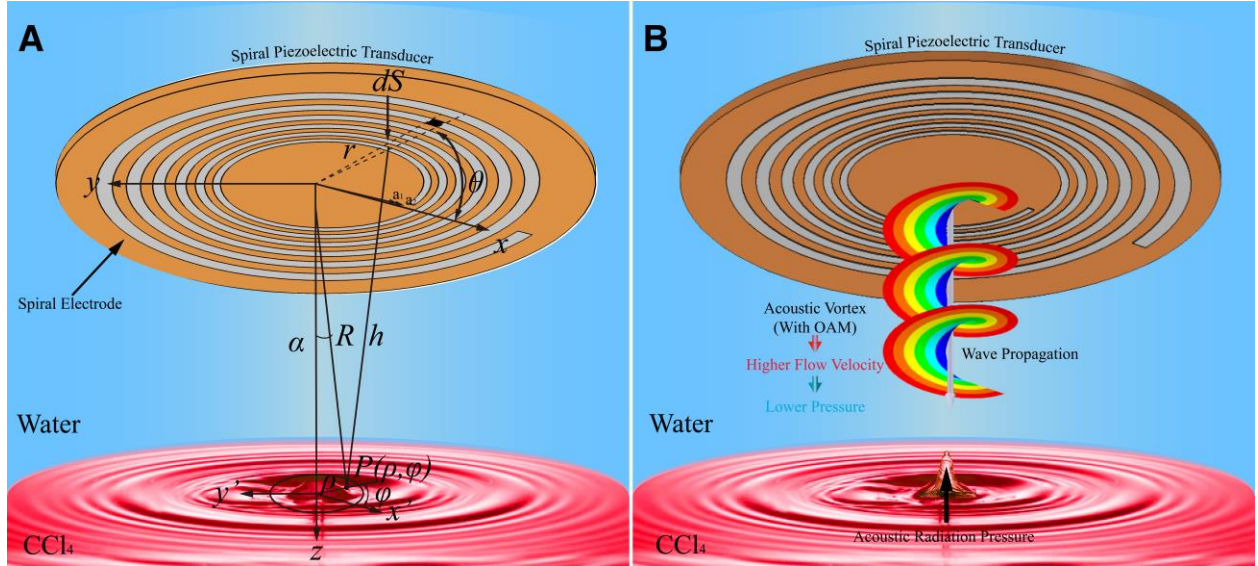


FIG. 1. Schematic diagram of the miniwatt spiral aspirators (a) cylindrical coordinate; (b) vortex acoustic field

According to the design of the spiral electrode on the surface of the transducer, the acoustic pressure field produced by the single spiral electrode transducer under the cylindrical coordinate can be expressed as,

$$p(\rho, \varphi, z) = v_a \rho_0 c_0 \int_0^{\theta_{\max}} \int_{a_1 e^{b\theta}}^{a_2 e^{b\theta}} \frac{i\omega\rho_0}{2h} e^{i(\omega t - kh)} r dr d\theta \quad (1)$$

where  $p$  represents the acoustic pressure at point  $P$  in the acoustic field,  $\rho$  represents the radial distance,  $\varphi$  represents the azimuth,  $z$  represents the axial distance,  $v_a$  represents amplitude,  $\rho_0$  and  $c_0$  represent the density and acoustic velocity of water,  $h\left(=\sqrt{\rho^2 + r^2 + z^2 - 2rR \cos \varphi \sin \alpha}\right)$  represents the distance of  $dS$  on spiral electrode to point  $P$ ,  $R\left(=\sqrt{\rho^2 + z^2}\right)$  represents the distance from the center of transducer surface to point  $P$  and  $\alpha$  represents the angle between the axis and the connection line of point  $P$  and the center of transducer surface. We integrated the whole area

of the spiral electrode, and the integral terms  $r$  and  $\theta$  in the integral equation represent the radius and azimuth of the  $dS$  on the spiral electrode, respectively.

The Brillouin's radiation stress tensor  $S_T$  under the cylindrical coordinates can be expressed as,

$$\mathbf{S}_T = (\langle K \rangle - \langle V \rangle) \mathbf{I} - \rho_0 \langle \mathbf{u}\mathbf{u} \rangle \quad (2)$$

where  $\langle \bullet \rangle$  represents the volume average of the corresponding quantities of the acoustic field in Fig. 1(a).  $K$  and  $V$  represent the kinetic energy and the potential energy, respectively.  $\mathbf{I}$  is the unit tensor, and  $\mathbf{u}$  is the particle vibration velocity at point P. According to the definition of the kinetic energy and the potential energy, the above expression can be calculated as,

$$\mathbf{S}_T = \left( \frac{\rho_0}{2} \langle \mathbf{u}^2 \rangle - \frac{1}{2\rho_0 c_0^2} \langle p^2 \rangle \right) \mathbf{I} - \rho_0 \langle \mathbf{u}\mathbf{u} \rangle \quad (3)$$

Then the radiation force resulting from the vortex acoustic field can be expressed as the integral of the Brillouin stress tensor,

$$F = \oint_A \mathbf{S}_T \cdot d\mathbf{A} = -\oint_A \rho_0 \langle \mathbf{u}\mathbf{u} \rangle \cdot d\mathbf{A} + \oint_A \left\{ \frac{\rho_0}{2} \langle |\mathbf{u}|^2 \rangle - \frac{1}{2\rho_0 c_0^2} \langle p^2 \rangle \right\} dA \quad (4)$$

From  $\mathbf{u} = \nabla\psi$  and  $p = \rho_0 \partial\psi / \partial t$ , the particle vibration velocity  $\mathbf{u}$  can be obtained by the acoustic pressure  $p$ , where  $\psi$  represents the velocity potential. Therefore, the solution of the radiation force depends on the expression of acoustic pressure generated by the single spiral-electrode transducer. The upper and lower limits of  $r$  are the outer radius and inner radius of the spiral electrode, respectively.

According to the study of the radiation force of the spiral Bessel beam by Marston [44], the axial radiation force  $F_z$  can be expressed as  $F_z = \pi\rho_0 k (I_3 - I_1 - I_2)$  (Supplementary I).  $I_1$  and  $I_2$  are the components obtained by the potential energy part in Eq. 3, respectively.  $I_3$  is the component of the

1  
2  
3  
4 product of velocity of particle vibration, and it can also be regarded as the component of the  
5  
6 product of velocity potential gradient. Since  $I_3$  has a positive effect on the axial radiation force,  
7  
8 that is, the larger the  $I_3$ , the greater the axial radiation force. The radiation force is negative when  
9  
10 extracting the liquid column at the two-phase liquid interface, so the larger  $I_3$  is, the smaller the  
11  
12 negative radiation force is.  $I_3$  is the component of the velocity potential gradient product. It is well  
13  
14 known that the acoustic field of the acoustic vortex is a kind of spiral acoustic wave, and there is  
15  
16 a certain angle in the acoustic wave direction. Compared with the ordinary plane wave moving in  
17  
18 a single direction, it will have a larger velocity potential gradient, so its radiation force could be  
19  
20 smaller.  
21  
22  
23  
24  
25  
26  
27  
28

### 29 **3. Experimental demonstration of precise extraction of droplets**

30  
31 Our experiment was carried out in a transparent cylindrical glass container with a height of  
32  
33 30 cm and a diameter of 20 cm, as shown in Fig. 2(b). The two kinds of liquids used in the  
34  
35 experiments are carbon tetrachloride ( $\text{CCl}_4$ , density  $\rho_1=1600 \text{ kg}\cdot\text{m}^{-3}$ , acoustic velocity  $c_1=926 \text{ m}\cdot\text{s}^{-1}$ )  
36  
37 and water (density  $\rho_2=1000 \text{ kg}\cdot\text{m}^{-3}$ , acoustic velocity  $c_2=1500 \text{ m}\cdot\text{s}^{-1}$ ). Because of  $\rho_1\cdot c_1\approx\rho_2\cdot c_2$ ,  
38  
39 the difference of acoustic impedance between the two liquids is very small, and acoustic waves  
40  
41 can pass through almost lossless. In terms of equipment, we use a signal generator to output low-  
42  
43 power RF signals and then use a power amplifier with a maximum magnification of 50 dB to gain  
44  
45 high-power RF signals that required for the transducer to work properly. The working power of  
46  
47 the piezoelectric transducer is also controlled by the signal generator. Oscilloscope was connected  
48  
49 to both ends of the transducers to better measure the real-time working voltage of the transducers  
50  
51 during the experiments. Except the measure of voltage, we combined the virtual instrument board  
52  
53 NI ELVIS  $\square+$  of NI Company and the digital multimeter on the computer to measure the high-  
54  
55  
56  
57  
58  
59  
60  
61  
62  
63  
64  
65



frequency current in the experimental circuit in real time. Due to the rapid process of the deformation of interface and extraction of droplets, we used a high-speed camera to shoot experimental phenomenon and computer to record videos in order to better observe and record the test phenomenon. In the experiment, the single spiral-electrode transducer is fixed in the upper water by a fixture, its side with the spiral electrode faces down and is parallel to the interface of the two-phase liquid, so as to emit acoustic vortex to the interface [Fig. 2(b)].

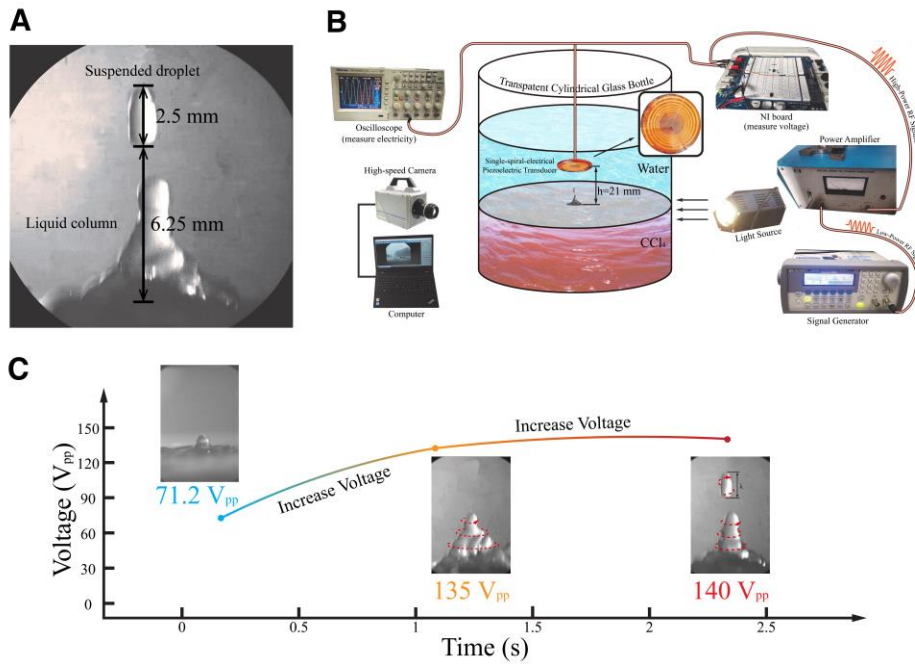


FIG. 2. The process of droplet appearance. (a) The liquid column extracted by spiral electrode transducer; (b) Schematic of experimental design and devices. (c) Process of extracting droplets by single spiral-electrode transducer.

According to the single spiral-electrode transducer used in our experiment, the inner radius of the spiral electrode is  $a_1 e^{b\theta}$ , the outer radius is  $a_2 e^{b\theta}$ , Where initial inner radius  $a_1 = 9$  mm, initial outer radius  $a_2 = 9.65$  mm and growth rate  $b = 0.0025$ . The range of  $\theta$  is 0 to  $12\pi$ , which means that the spiral electrode rotates 6 times totally.

Since the single vortex is the most basic and stable structure in all acoustic vortex, we used a

1  
2  
3  
4 single spiral-electrode transducer [Fig. S1] which can produce single vortex. In the experiment,  
5  
6 we successfully realized the deformation of the interface of two-phase liquid at 608.3 kHz [Fig.  
7  
8 2(c)]. At this time, the distance between the lower face of the transducer and the liquid level is 21  
9  
10 mm, the working voltage is 71.2 V<sub>pp</sub>, the current is 0.27 A, and the power is 6.8 W. After the single  
11  
12 spiral-electrode transducer successfully aspirating the CCl<sub>4</sub> liquid column, we increased the  
13  
14 voltage applied to the transducer, and the height of the liquid column increased as the voltage goes  
15  
16 up. When the working voltage of the transducer increases to 140V<sub>pp</sub>, the top of the liquid column  
17  
18 becomes unstable and separated independent CCl<sub>4</sub> droplet. After maintaining the voltage for about  
19  
20 1 s, the single spiral-electrode transducer successfully captured the independent droplets detached  
21  
22 from the liquid column and suspending them stably in the water layer, as shown in Fig 2(a). At  
23  
24 this time, the working voltage of the transducer is 140V<sub>pp</sub>, the current is 0.8A and the power is  
25  
26 39.6W. The droplets captured in the experiment are oval, the length of the major axis is 2.5mm  
27  
28 and the length of the minor axis is 1.2mm. The size of droplet is close to the wavelength of acoustic  
29  
30 waves in water (2.46mm), and the volume of droplet is about 1.9mm<sup>3</sup>. We have effectively proved  
31  
32 the feasibility of the droplet aspirator through experiments. The droplet aspirator based on acoustic  
33  
34 vortex shows an ideal working state from promoting the deformation on the liquid interface at low  
35  
36 voltage to accurately capturing and manipulating suspended droplets at high voltage. In order to  
37  
38 further illustrate the unique advantages of our designed system, we combined with simulations to  
39  
40 explain the significant advantages of our droplet aspirator based on acoustic vortex in liquid  
41  
42 extraction and capture through the calculation of acoustic field and power.  
43  
44  
45  
46  
47  
48  
49  
50  
51  
52

53 In addition to the theoretical calculation, we also combined it with the COMSOL simulations  
54  
55 to further research the acoustic field of the transducer. The working frequency of the transducer in  
56  
57 simulation is 608.3kHz. According to the simulation results, we calculate the acoustic power at the  
58  
59  
60  
61  
62  
63  
64  
65

1  
2  
3  
4 surface of the transducer, which is 2.61 W. The power of 2.61 W we use by vortex beams is less  
5 than a power of 7.2 W used in [45] by focused beams.  
6

7  
8 According to Eq. 4, we can solve the radiation force produced by the single spiral-electrode  
9  
10 transducer on the liquid interface combined with the simulation results. When the parameters in  
11 the simulation results are brought into the solution equation of the radiation force, the time average  
12 of the parameter product in the equation can be expressed as the product of the corresponding first  
13 complex number and the corresponding second conjugate complex number.  
14  
15  
16  
17  
18  
19  
20

$$21 \quad P_r = -\rho_0 (\mathbf{u}\mathbf{u}^*) + \frac{\rho_0}{2} (|\mathbf{u}\|\mathbf{u}^*|) - \frac{1}{2\rho_0 c_0^2} (pp^*) \quad (5)$$

22  
23  
24  
25 According to the Eq. (5), we can obtain the distribution diagram of  $|P_r|$  at the interface of  
26 two-phase liquid. At the same time, we also add the simulation results of the ordinary circular  
27 electrode transducer without spiral-electrode, to compare the  $|P_r|$  generated by the two transducers  
28 on the liquid interface [Fig. 3(a)]. Due to non-spiral transducer has a larger electrode area which  
29 lead to larger current at the same voltage, the working power of transducer will be larger. In order  
30 to maintain the same working power of two kinds of transducer during the comparison, we reduce  
31 the simulation voltage of the non-spiral transducer (Supplementary IV).  
32  
33  
34  
35  
36  
37  
38  
39  
40  
41

42 However, in the experiment, we found that at the same working power, the focused beam  
43 produced by the non-spiral transducer is not as effective as the single spiral transducer in extracting  
44 droplets. Therefore, it shows that the acoustic vortex does not only rely on the acoustic radiation  
45 force when extracting the droplet, and the biggest difference between the focused beam and the  
46 acoustic vortex is whether it carries angular momentum or not. Therefore, the angular momentum  
47 carried by the acoustic vortex plays an important role in the process of extracting droplets.  
48  
49  
50  
51  
52  
53  
54  
55  
56  
57  
58  
59  
60  
61  
62  
63  
64  
65

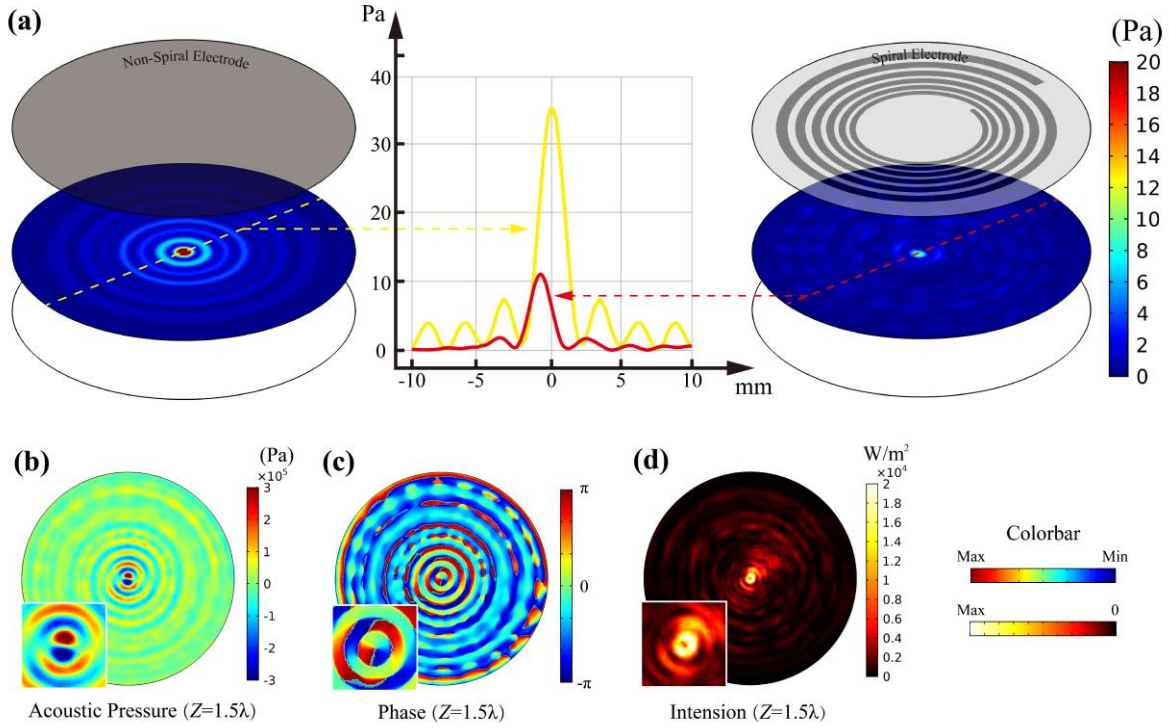


FIG. 3. Comparison of acoustic radiation forces and diagram of acoustic vortex beams (a) Comparison of acoustic radiation pressure at the interface between non-spiral electrode and single spiral electrode transducers; (b, c and d) The acoustic pressure, phase and intensity at 1.5 wavelengths from the surface of the spiral transducer with the cross-sectional views.

Actually, the vortex can be regarded as the winding and superposition of two acoustic beams with phase difference of  $\pi$ . We can better observe the special acoustic field of the vortex by observing the cross-section on the z-axis. Here, we intercept the plane distribution diagram of various acoustic field parameters at 1.5 wavelengths (3.7mm) from the transducer. From the cross-sectional view of the acoustic pressure, we can see that there are both positive and negative acoustic pressure in the center of the section, and the symbol of the two acoustic pressure are opposite [Fig. 3(b)], which represent the two acoustic beams with a phase difference of  $\pi$ . According to the cross-section of phase, we can see that the phase obviously makes a jump from

1  
2  
3  
4  $\pi$  to  $-\pi$  [Fig. 3(c)], which is also the unique phase feature of the acoustic vortex. Finally, we also  
5  
6 give the cross-sectional view of the acoustic field intensity [Fig. 3(d)], and the distribution diagram  
7  
8 of acoustic pressure intensity is the time average of the acoustic intensity. It can be seen that a  
9  
10 bright ring is formed in the center of the intensity field, and there is a small part of the zero intensity  
11  
12 region at the center of the bright ring, which is due to the acoustic pressure offset at the center of  
13  
14 the two beams with a difference of  $\pi$  in the vortex. Here, we introduce the distribution diagram of  
15  
16 acoustic pressure, phase and intensity in the acoustic field of a single spiral-electrode transducer.  
17  
18 It is explained from many aspects that the single spiral-electrode transducer can effectively  
19  
20 produce the acoustic vortex with smaller radiation force.  
21  
22  
23  
24

25  
26 Zhang et al analyzed and studied the transfer of OAM [46] and OAM carried by the acoustic  
27  
28 vortex. Here, we further analyze the mechanism of lifting the liquid column of the spiral transducer  
29  
30 based on the loss of angular momentum of the acoustic vortex and the Bernoulli principle. The  
31  
32 Bernoulli equation can be expressed as,  
33  
34

$$P_h + \frac{1}{2} \rho v^2 + \rho gh = C \quad (6)$$

35  
36  
37  
38  
39  
40 In Eq. (6),  $P_h$  represents the pressure at a certain point,  $v$  is the fluid velocity at the change  
41  
42 point,  $\rho$  is the fluid density,  $h$  is the height at that point, and  $C$  is a constant. This equation can be  
43  
44 explained in a more easy-to-understand way: where the flow rate is fast, the pressure is low, and  
45  
46 where the velocity is low, the pressure is high.  
47  
48

49  
50 In our experiment of extracting liquid droplets, the acoustic radiation pressure produced by  
51  
52 acoustic waves at the interface of two-phase liquid needs to overcome not only the surface tension  
53  
54 of the liquid interface, but also the pressure given by the upper liquid. When the acoustic vortex  
55  
56 produced by a single spiral-electrode transducer propagates in the upper water, the angular  
57  
58 momentum carried by the acoustic vortex will be transferred to the water supply, thus speeding up  
59  
60  
61  
62

the flow speed of the water. Then, according to Bernoulli's law, when the velocity of water increases, the pressure of the upper water on the interface of the two-phase liquid will decrease, so under the action of acoustic radiation pressure, the liquid interface is more likely to deform and form a protruding liquid column. Therefore, the acoustic vortex produced by the transducer will affect the velocity and pressure of the upper liquid through the exchange of angular momentum. The magnitude of angular momentum can be calculated according to Eq. (7).

$$\langle \dot{L}_z \rangle = \frac{m \cdot P}{\omega_B} \quad (7)$$

where  $m$  represents the topological charge of the acoustic vortex,  $P$  represents the acoustic power, and  $\omega_B$  represents the angular frequency of the acoustic beam. Therefore, there is no angular momentum in the transducer without spiral, that is, the acoustic beam produced by  $m \neq 0$ , and only the acoustic vortex with  $m \neq 0$  carries angular momentum.

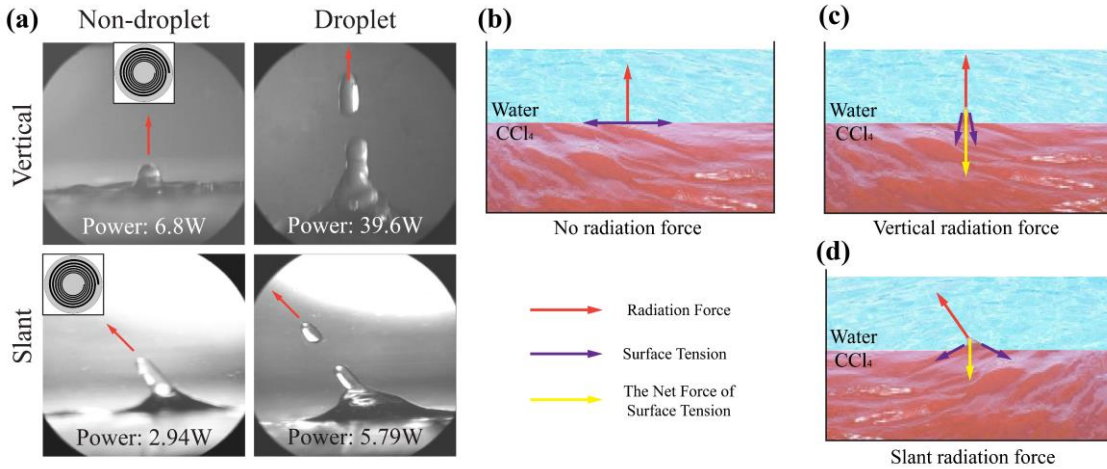


FIG. 4. The result when single spiral-electrode transducer is slant. (a) Power comparison of vertical and slant transducers in extraction column and droplet extraction; (b, c and d) Schematic diagram of force analysis when no force, vertical force and slant force applied on liquid level.

Through the surface integration in the simulation, we can get the acoustic power of the spiral

1  
2  
3  
4 transducer at different axial distances from the upper liquid medium. We calculate the angular  
5  
6 momentum of the acoustic vortex at different positions in the upper liquid according to the acoustic  
7  
8 power of the acoustic beam. According to the simulation and calculation results, the variation of  
9  
10 the acoustic power and angular momentum of the acoustic vortex with the axial distance can be  
11  
12 obtained [Fig. S5]. When the axial distance increase, the angular momentum of the vortex is  
13  
14 obviously smaller, which is due to the angular momentum transfer between the vortex and the  
15  
16 liquid medium. It is precisely because the angular momentum transfer of the acoustic vortex, the  
17  
18 velocity of the water layer increases and the pressure decreases greatly. So, compared with the  
19  
20 non-spiral transducer, the single spiral-electrode transducer can lift the liquid column more easily.  
21  
22  
23  
24  
25

26 In the experiment, we find that when the angle between the axis of the transducer and the  
27  
28 interface of two-phase liquid is  $45^\circ$ , the liquid column can also be extracted at the interface of two-  
29  
30 phase liquid. The liquid column is no longer vertical, but has a certain inclination, and the top of  
31  
32 the liquid column always faces the transducer. As shown in Fig. 4(a), we show the comparison  
33  
34 results of the working power of extracting the liquid column and droplets when transducers  
35  
36 working vertically and obliquely. It is obvious that when the transducer is tilted, the liquid column  
37  
38 and droplets can be extracted with less working power.  
39  
40  
41  
42

43 In this regard, we did a simple force analysis. When the acoustic radiation force first started  
44  
45 to apply on the horizontal liquid interface, the surface tension produced on both sides of the point  
46  
47 where transducer put radiation force on, and the radiation force is in the horizontal direction [Fig.  
48  
49 4(b)]. Due to the surface tension has no component in the vertical direction, it will not hinder the  
50  
51 production of the liquid column.  
52  
53  
54

55 When the liquid column is produced, the liquid interface shows raised state. Because the  
56  
57 surface tension is always along the direction of liquid interface [Fig. 4(c)], it will produce  
58  
59  
60  
61

1  
2  
3  
4 downward surface tension along both sides of the liquid column. There is a vertical resultant force  
5  
6 of the surface tension which is opposite to the direction of the radiation force, it will hinder the  
7  
8 extraction of the liquid column.  
9

10  
11 When the slant transducer put radiation force on the liquid interface, the liquid column is slant  
12  
13 because the radiation force will produce not only the vertical force, but also the horizontal force.  
14  
15 It can be seen that the slant liquid column is smoother and the angle in the horizontal direction is  
16  
17 smaller. It is more conducive that extract the liquid column, because the vertical resultant force of  
18  
19 the surface tension is obviously reduced [Fig. 4(d)].  
20  
21  
22

23  
24 Here, we report a new kind of miniwatt aspirators which can accurately capture and  
25  
26 manipulate wavelength-sized droplets. Inspired by the special spiral dynamic mechanism, we  
27  
28 apply the acoustic vortex with OAM to the precise droplet capture and control in two-phase liquid  
29  
30 for the first time. Through experiments, we use the acoustic vortex generated by single spiral-  
31  
32 electrode transducer to extract droplets from the interface of two-phase liquids. Compared with  
33  
34 the focused beam, the acoustic vortex can realize the extraction of wave droplets with less acoustic  
35  
36 radiation force.  
37  
38  
39  
40  
41  
42

#### 43 **4. Conclusion**

44  
45 At present, the liquid-liquid two-phase fluid has a great advantage in droplet extraction  
46  
47 because of its low impedance and small loss of acoustic waves when it penetrates the interface.  
48  
49 However, there is no related research on the contactless extraction of droplets at the interface of  
50  
51 two-phase fluids with higher impedance, such as liquid-gas. Due to the increase of the impedance  
52  
53 of the two-phase interface, the droplet aspirator based on acoustic vortex is expected to break  
54  
55 through the shackles of the gas-liquid interface to extract droplets. Miniwatt droplet aspirator has  
56  
57  
58  
59  
60  
61  
62  
63  
64  
65



1  
2  
3  
4 very important application value in chemical industry, medicine and other fields [47]. This special  
5  
6 spiral structure is expected to be used in bio-inspired piezoelectric materials.  
7  
8  
9

## 10 11 **APPENDIX A: MANUFACTURE OF SPIRAL PIEZOELECTRIC TRANSDUCER**

12  
13  
14 Our piezoelectric transducers are made from 25-mm radius and 1-mm thick PZT-4. We gave  
15  
16 the thread model file drawn by COMSOL to the factory for electrode coating, with one side as  
17  
18 spiral electrode and the other as fully coated electrode. After the electrode coating is completed,  
19  
20 we need weld wires on both sides of the electrode as the input and output terminals of the  
21  
22 transducers. Generally, the input terminal (red wire) is the spiral electrode and the output end  
23  
24 (black wire) is the fully coated electrode. The thread of single spiral piezoelectric transducer can  
25  
26 be directly welded to the wire. Since there are multiple threads in the multi-spiral piezoelectric  
27  
28 transducer, it is necessary to first connect the threads through the wires in series and then weld the  
29  
30 input terminal. Finally, the transducer that completes port welding can be made by gluing.  
31  
32  
33  
34  
35

## 36 **APPENDIX B: THE EXPERIMENTAL DEVICES**

37  
38  
39 In the experiments, we provided RF AC signals through Agilent 32210A function signal  
40  
41 generator, and then used MODEL 2100L RF power amplifier with maximum voltage gain of 50  
42  
43 dB and frequency range of 10 kHz ~ 12 MHz for power amplification. Tektronix TDS2024B  
44  
45 oscilloscope was used to measure the voltage at both ends of the transducer. The NI board used to  
46  
47 measure the high-frequency current in the circuit is NI ELVIS II+.  
48  
49  
50

## 51 **APPENDIX C: THE USE OF HIGH-SPEED CAMERA**

52  
53  
54 We used Photron's FASTCAM SA1.1 high-speed camera to record the experiments. The  
55  
56 camera is connected to a computer with a gigabit-nic through a cable, and the computer's IP address  
57  
58 needs to be set correctly according to the camera manual. It is necessary to install the camera  
59  
60  
61  
62  
63  
64  
65

1  
2  
3  
4 software PFV on the computer to control the camera for photographing and recording. Since we  
5  
6 are used a black and white lens, we need to place a light source aimed at the camera lens to get the  
7  
8 picture. In our experiments, the shooting frame rate of high-speed video was 5400 fps and the  
9  
10 resolution was 1024×1024.  
11  
12

### 13 14 15 16 **Declaration of competing interest**

17  
18 None.  
19  
20  
21  
22

### 23 **Acknowledgements**

24  
25  
26 We acknowledge Professor Jianchun Wang from Southern University of Science and  
27  
28 Technology for his valuable suggestions on the part of our experimental analysis about Bernoulli's  
29  
30 theorem. And we thank Robert Lirette and Likun Zhang for discussions by email. Funding: We  
31  
32 also acknowledge support from the National Natural Science Foundation of China (Grant  
33  
34 Nos.11772349 and 11972354). Author contributions: H.Z. conceived the idea.  
35  
36

37 H.Z., J.Y., G.Z. and Y.L. built up the whole system. H.Z. and J.Z. designed all the experiments.  
38

39 H.Z., Y.Z. and Y.C. carried out the corresponding numerical simulations. Y.Z. and B.B.  
40

41 experimented and filmed all the scenes with the high-speed camera for the shooting. H.Z. and Y.Z.  
42

43 contributed to the scientific presentation. All the authors approved the final version of the  
44

45 manuscript. Competing interests: All other authors declare that they have no competing interests.  
46  
47

48  
49 Data and materials availability: All data needed to evaluate the conclusions in the paper are present  
50

51 in the paper and/or the Supplementary Materials. Additional data related to this paper may be  
52

53 requested from the authors.  
54  
55  
56  
57  
58  
59  
60  
61  
62  
63  
64  
65

## References

1. D. Foresti, K. T. Kroll, R. Amisshah, F. Sillani, K. A. Homan, D. Poulikakos and J. A. Lewis, Acoustophoretic printing, *Sci. Adv.* **4**, eaat1659 (2018).
2. H. Li, W. Fang, Y. Li, Q. Yang, M. Li, Q. Li, X. Feng and Y. Song, Spontaneous droplets gyrating via asymmetric self-splitting on heterogeneous surfaces, *Nat. Commun.* **10**, 950 (2019).
3. H. Li, W. Fang, Z. Zhao, A. Li, Z. Li, M. Li, Q. Li, X. Feng and Y. Song, Droplet precise self-splitting on patterned-adhesive surfaces for simultaneous multi-detection, *Angew. Chem.* **55**, 10535-10539 (2020).
4. W. Xu, H. Zheng, Y. Liu, X. Zhou, C. Zhang, Y. Song, X. Deng, M. Leung, Z. Yang, R. X. Xu, Z. Wang, X. Zeng and Z. Wang, A droplet-based electricity generator with high instantaneous power density, *Nat.* **578**, 392-396 (2020).
5. Y. Zhao, Z. Xu, H. Niu, X. Wang and T. Lin, Magnetic Liquid Marbles: Toward “Lab in a Droplet”, *Adv. Funct. Mater.* **25**, 437-444 (2014).
6. Y. Zheng, Z. Wu, M. Khan, S. Mao, K. Manibalan, N. Li, J.-M. Lin and L. Lin, Multi-functional Regulation of 3D Cell-laden Microspheres Culture on an Integrated Microfluidic Device, *Anal. Chem.* **91**, 12283-12289 (2019).
7. Z. Tian, S. Yang, P.-H. Huang, Z. Wang, P. Zhang, Y. Gu, H. Bachman, C. Chen, M. Wu, Y. Xie and T. J. Huang, Wave number–spiral acoustic tweezers for dynamic reconfigurable manipulation of particles and cells, *Sci. Adv.* **5**, eaau6062 (2019).
8. M. Baudoin, J.-C. Gerbedoen, A. Riaud, O. B. Mater, N. Smagin and J.-L. Thomas, Folding a focalized acoustical vortex on a flat holographic transducer: Miniaturized selective acoustical tweezers, *Sci. Adv.* **5**, eaav1967 (2019).

- 1  
2  
3  
4 9. Z. Tian, Z. Wang, P. Zhang, T. D. Naquin, J. Mai, Y. Wu, S. Yang, Y. Gu, H. Bachman, Y.  
5  
6 Liang, Z. Yu and T. J. Huang, Generating multifunctional acoustic tweezers in Petri dishes  
7  
8 for contactless, precise manipulation of bioparticles, *Sci. Adv.* **6**, eabb0494 (2020).  
9  
10  
11 10. D. Zang, J. Li, Z. Chen, Z. Zhai, X. Geng and B. P. Binks, Switchable Opening and Closing  
12  
13 of a Liquid Marble via Ultrasonic Levitation, *Langmuir* **31**, 11502-11507 (2015).  
14  
15  
16 11. D. Zang, L. Li, W. Di, Z. Zhang, C. Ding, Z. Chen, W. Shen, B. P. Binks and X. Geng,  
17  
18 Inducing drop to bubble transformation viaresonance in ultrasound, *Nat. Commun.* **9**, 3546  
19  
20 (2018).  
21  
22  
23 12. D. Guo, J. Xiao, J. Chen, Y. Liu, C. Yu, M. Cao and L. Jiang, Superhydrophobic “Aspirator”:  
24  
25 Toward Dispersion and Manipulation of Micro/Nanoliter Droplets, *Small* **11**, 4491-4496  
26  
27 (2015).  
28  
29  
30  
31 13. H. Dai, Z. Dong and L. Jiang, Directional liquid dynamics of interfaces with  
32  
33 superwettability, *Sci. Adv.* **6**, eabb5528 (2020).  
34  
35  
36 14. B. Su, S. Wang, Y. Song and L. Jiang, A Miniature Droplet Reactor Built on Nanoparticle-  
37  
38 DerivedSuperhydrophobic Pedestals, *Nano Res.* **4**, 266-273 (2011).  
39  
40  
41 15. Q. Shi, W. Di, D. Dong, L.W.Yap, L. Li, D.Zang and W. Cheng, A General Approach to  
42  
43 Free-Standing NanoassembliesviaAcoustic Levitation Self-Assembly, *ACS Nano* **13**, 5243-  
44  
45 5250 (2019).  
46  
47  
48 16. D. G. Grier, Optical tweezers in colloid and interface science. *Curr. Opin. Colloid In.* **2**, 264-  
49  
50 270 (1997).  
51  
52  
53 17. H. Kriegs, G. Petekidis, G. Fytas, R. S. Penciu, E. N. Economou and A. B. Schofield,  
54  
55 Phonons in suspensions of hard sphere colloids: Volume fraction dependence, *J. Chem. Phys.*  
56  
57 **121**, 7849-7854 (2004).  
58  
59  
60  
61  
62  
63  
64  
65

- 1  
2  
3  
4 18. R. G. Joshi, K. K. Mishra, V. Sivasubramanian and B.V.R. Tata, Anomalous behavior of  
5  
6 acoustic phonon in dense thermo-responsive microgel suspension studied using Brillouin  
7  
8 scattering, *Curr. Appl. Phys.* **16**, 1395-1402 (2016).  
9  
10  
11 19. E. Bormashenko, New insights into liquid marbles, *Soft Matter* **8**, 11018-11021 (2012).  
12  
13 20. Lord Rayleigh F. R. S, On the pressure of vibrations, *Philos. Mag.* **3**, 338-346 (1902).  
14  
15 21. S. Chu, L. Hollberg, J. E. Bjorkholm, A. Cable and A. Askin, Three-Dimensional Viscous  
16  
17 Confinement and Cooling of Atoms by Resonance Radiation Pressure, *Phys. Rev. Lett.* **55**, 48-  
18  
19 51 (1985).  
20  
21  
22 22. A. Ashkin, J. M. Dziedzic, J. E. Bjorkholm and S. Chu, Observation of a single-beam gradient  
23  
24 force optical trap for dielectric particles, *Opt. Lett.* **11**, 288-290 (1986).  
25  
26  
27 23. K. C. Neuman and A. Nagy, Single-molecule force spectroscopy: optical tweezers, magnetic  
28  
29 tweezers and atomic force microscopy, *Nat. Meth.* **5**, 491–505 (2008).  
30  
31  
32 24. F. Guo, P. Li, J. B. French, Z. Mao, H. Zhao, S. Li, N. Nama, J. R. Fick, S. J. Benkovic and  
33  
34 T. J. Huang, Controlling cell–cell interactions using surface acoustic waves, *PNAS.* **112**, 43-  
35  
36 48 (2015).  
37  
38  
39 25. C. R. P. Courtney, C. E. M. Demore, H. Wu, A. Grinenko, P. D. Wilcox, S. Cochran and B.  
40  
41 W. Drinkwater, Independent trapping and manipulation of microparticles using dexterous  
42  
43 acoustic tweezers, *Appl. Phys. Lett.* **104**, 154103 (2014).  
44  
45  
46 26. J. Wu, Acoustical tweezers, *J. Acoust. Soc. Am.* **89**, 2140-2143 (1991).  
47  
48  
49 27. M. Baudoin and J.-L. Thomas, Acoustic Tweezers for Particle and Fluid Micromanipulation,  
50  
51 *Annu. Rev. Fluid Mech.* **52**, 205-234 (2019).  
52  
53  
54 28. D. Baresch, J.-L. Thomas and R. Marchiano, Three-dimensional acoustic radiation force on  
55  
56 an arbitrarily located elastic sphere, *J. Acoust. Soc. Am.* **133**, 25-36 (2013).  
57  
58  
59  
60  
61  
62  
63  
64  
65

- 1  
2  
3  
4 29. D. Baresch, J.-L. Thomas and R. Marchiano, Observation of a single-beam gradient  
5  
6 forceacoustical trap for elastic particles: Acoustical tweezers, *Phys. Rev. Lett.* **116**, 024301  
7  
8 (2016).  
9
- 10  
11 30. Z. Cai, Z. Huang, Z. Li, M. Su, Z. Zhao, F. Qin, Z.Zhang, J. Yang and Y. Song, Evaporation  
12  
13 Induced Spontaneous Micro-Vortexes via Engineering Marangoni Flow, *Angew. Chem. Int.*  
14  
15 *Ed.* **52**, 23892-23897 (2020).  
16  
17
- 18  
19 31. O. D. Velev and K. H. Bhatt, On-chip micromanipulation and assembly of colloidal particles  
20  
21 by electric fields, *Soft Matter* **2**, 738-750 (2006).  
22
- 23  
24 32. K. H. Bhatt, S. Grego and O. D. Velev, An AC Electrokinetic Technique for Collection and  
25  
26 Concentration of Particles and Cells on Patterned Electrodes, *Langmuir* **21**, 6603-6612  
27  
28 (2005).  
29
- 30  
31 33. J. Harte, A. Kinzig and J. Green, Self-similarity in the distribution and abundance of species,  
32  
33 *Sci.* **284**, 334–336 (1999).  
34
- 35  
36 34. V J. Paul, A review of geometry investigations of helicoids, *IOP Conf. Series: Materials*  
37  
38 *Science and Engineering* **371**, 012029 (2018).  
39
- 40  
41 35. J. W. Cohen, “On stress calculations in helicoidal shells and propeller blades,” doctoral  
42  
43 thesis, Delft University of Technology (1995).  
44
- 45  
46 36. D. W. Taylor, *The Speed and Power of Ships* (Press of Ransdell, WashingtonD.C., 1933), p.  
47  
48 130.  
49
- 50  
51 37. Y. M. Grigorenko, V. I. Gulyaev, E. A. Gotsulyak and K. Ashuri, Stress-strain state of  
52  
53 tubular shells under uniform surface pressure, *Soviet Applied Mechanics* **19**, 656-662 (1983).  
54
- 55  
56 38. B. Issenmann, R. Wunenburger and J. P. Delville, Deformation of acoustically transparent  
57  
58 fluid interfaces by the acoustic radiation pressure, *EPL.* **83**, 34002 (2008).  
59  
60  
61  
62  
63  
64  
65

- 1  
2  
3  
4 39. R. W. Wood and A. L. Loomis, The physical and biological effects of high-frequency sound-  
5 waves of great intensity, *Journal of the Franklin Institute* **205**, 151-153 (1928).  
6  
7  
8  
9 40. G. Hertz and H. Mende, Der Schallstrahlungsdruck in Flüssigkeiten, *Zeitschrift für Physik*  
10 **114**, 354-367 (1939).  
11  
12  
13  
14 41. J. L. Ealo, J. C. Prieto and F. Seco, Airborne ultrasonic vortex generation using flexible  
15 ferroelectrics, *IEEE Trans. Ultrason. Ferroelectr. Freq. Control* **58**, 1651-1657 (2011).  
16  
17  
18  
19 42. X. Jiang, Y. Li, B. Liang, J. Cheng and L. Zhang, Convert Acoustic Resonances to Orbital  
20 Angular Momentum, *Phys. Rev. Lett.* **117**, 034301 (2016).  
21  
22  
23  
24 43. H. Tang, Z. Chen, N. Tang, S. Li, Y. Shen, Y. Peng, X. Zhu and J. Zang, Hollow-Out  
25 Patterning Ultrathin Acoustic Metasurfaces for Multifunctionalities Using Soft fiber/Rigid  
26 Bead Networks, *Adv. Funct. Mater.* **36**, 1801127 (2018).  
27  
28  
29  
30  
31 44. P. L. Marston, Scattering of a Bessel beam by a sphere: II. Helicoidal case and spherical shell  
32 example, *J. Acoust. Soc. Am.* **124**, 2905-2910 (2008).  
33  
34  
35  
36 45. R. Lirette, J. Mobley and L. Zhang, Ultrasonic Extraction and Manipulation of Droplets from  
37 a Liquid-Liquid Interface with Near-Field Acoustic Tweezers, *Phys. Rev. Lett.* **12**, 061001  
38 (2019).  
39  
40  
41  
42  
43 46. L. Zhang and P. L. Marston, Angular momentum flux of nonparaxial acoustic vortex beams  
44 and torques on axisymmetric objects, *Phys. Rev. E* **84**, 065601 (2011).  
45  
46  
47  
48 47. K. Cohen, *The Theory of Isotope Separation as Applied to the Large-Scale Production of*  
49 *U235*, (McGraw-Hill, 1951), p. 103.  
50  
51  
52  
53  
54  
55  
56  
57  
58  
59  
60  
61  
62  
63  
64  
65